Polymer Journal (2019) 51:275–281
https://doi.org/10.1038/s41428-018-0149-0

ORIGINAL ARTICLE

# Dispersion state of carbon black in polystyrene produced with different dispersion media and its effects on composite rheological properties

Yudai Fukunaga[1] · Yoshihisa Fujii[2] · Seisuke Inada[3] · Yoshihiro Tsumura[3] · Mitsunori Asada[3] · Masanobu Naito[4] · Naoya Torikai[1,2]

Received: 20 August 2018 / Revised: 5 October 2018 / Accepted: 9 October 2018 / Published online: 16 November 2018


**Abstract**

The dispersion state and aggregate structure of carbon black in polystyrene composites prepared by solvent casting suspensions in different dispersion media, i.e., chloroform, tetrahydrofuran, and toluene, with different particle contents and their effects on the bulk rheological properties of the composites were investigated by transmission electron microscopy, ultrasmall-angle and small-angle X-ray scattering, and dynamic viscoelasticity measurements. The macroscopic dispersion state of carbon black in the solvent-cast films was largely affected by the dispersion medium, reflecting the stability of the suspension in the polystyrene solution. The mass fractal dimension of carbon black in the polymeric matrix, which was evaluated by X-ray scattering techniques with a resolution of nanometers, tended to exhibit a higher value for the dispersion media with less carbon black dispersibility. The surface fractal dimension of carbon black in the polymer was independent of the dispersion medium and exhibited a lower value than carbon black powder due to physical adsorption of the polymer on the particle surface. The viscoelastic moduli for the melt polymer composites below and above the percolation limit varied according to the dispersion media, reflecting the difference in the macroscopic dispersion state and aggregate structure of carbon black in polystyrene.

## Introduction

Recently, a polymer composite with solid particles has attracted attention as a promising material due to its high mechanical strength and high functionality, and its utilization has been extended to a variety of applications such as tire materials [1, 2]. The physical properties and functions of a polymer composite are influenced not only by the respective constituent materials but also by the dispersion state and aggregate structure of the particles in the polymeric matrix. Therefore, to control the physical properties and functions of these composites, the structure and physical properties of a polymer composite must be understood.

The small-angle scattering techniques of light, X-ray, and neutrons are very powerful tools for the structural analysis of particles dispersed in a solvent or polymer on a nanometer scale [3, 4]. One of the advantages of small-angle scattering techniques is that they are nondestructive, so in situ and time-resolved measurements are applicable. Particles such as fumed silica and carbon black (CB) possess hierarchical structures with aggregates composed of primary particles with sizes of a few tens of nanometers. The mass and surface fractal dimensions of these

✉ Naoya Torikai
ntorikai@chem.mie-u.ac.jp

[1] Graduate School of Regional Innovation Studies, Mie University, 1577 Kurimamachiya, Tsu, Mie 514-8507, Japan

[2] Department of Chemistry for Materials, Graduate School of Engineering, Mie University, 1577 Kurimamachiya, Tsu, Mie 514-8507, Japan

[3] Kurashiki Research Center, Kuraray Co., Ltd., 2045-1 Sakazu, Kurashiki, Okayama 710-0801, Japan

[4] Research and Services Division of Materials Data and Integrated System (MaDIS), National Institute for Materials Science (NIMS), 1-2-1 Sengen, Tsukuba, Ibaraki 305-0047, Japan

particles have been evaluated in suspensions and polymer composites by using small-angle scattering techniques [5–13]. As a more advanced method, Qiu et al. [14–17], Takenaka et al. [18], and Song et al. [19] extracted structural information on polymer chains bound to particles in suspensions and composites by neutron small-angle scattering with contrast variation.

To date, there have been several studies on the rheological properties and particle dispersibility of suspensions [20–23] and polymer composites [24–33] with various combinations of dispersion media and particles. Filippone et al. [29] investigated the relationships between structure and linear viscoelasticity for polystyrene (PS)/fumed silica composites with different particle contents, and the critical particle volume fraction, $\phi_c$, for percolation was evaluated to be ~2%. Above $\phi_c$, the elasticity of the space-filling network of the particles dominates the storage modulus at a low angular frequency. The value of $\phi_c$ varies according to the particle and its interaction with the matrix polymer [30]. Capuano et al. [31] examined the linear viscoelasticity of a composite of poly(ethylene oxide) (PEO) and fumed silica with respect to the difference in the dispersion state of the particles in a polymer matrix produced by melt compounding and freeze drying. They indicated that the viscoelasticity was higher for the composite prepared by freeze drying than the composite prepared by melt compounding.

In general, a polymer composite is fabricated by mechanical compounding at high temperatures above the melting point of the polymer in practical use, and the dispersion state of particles in a polymer matrix is determined by the mechanical conditions of the compounding. On the other hand, the stability of a suspension in a polymer solution acting as a dispersion medium is controllable by various colloidal interactions such as van der Waals interactions, steric interactions of the adsorbed polymer, depletion interactions, etc. [34]. Different dispersion states of particles in a composite can be easily produced by solvent casting a suspension in a polymer solution [35].

In this study, the relationships between the dispersion state of carbon black (CB) in PS and the rheological properties of the melt polymer composite with CB were examined on composite films prepared by solvent casting suspensions in different dispersion media. The dispersion state and aggregate structure of CB in PS were observed by transmission electron microscopy (TEM) and a combination of ultrasmall-angle and small-angle X-ray scattering (USAXS and SAXS), and the rheological properties of the composites were investigated by dynamic viscoelasticity measurements at a temperature above the glass transition temperature.

## Materials and methods

### Materials

The CB used in this study was kindly supplied by Mitsubishi Chemical Corporation, and its primary particle diameter and specific surface area are 16 nm and 260 $m^2/g$, respectively. The matrix polymer for the composite was atactic polystyrene with a number-averaged molecular weight of $100 \times 10^3$ and polydispersity of 1.06, and was purchased from Polymer Source, Inc. Chloroform, THF, and toluene with a grade of ∞ pure from FUJIFILM Wako Pure Chemical Corporation were used as the dispersion media without further purification.

The CB was dispersed in each dispersion medium by ultrasonication at 420 W for 1 h using an ultrasonic dispersion apparatus (UH-600S of SMT Co., Ltd.), and then was mixed with the separately prepared PS solution to make a CB suspension in a 0.02 g/mL PS solution. This concentration roughly corresponds to the critical overlap concentration of the polymer. The added amounts of CB were 2.7 and 10% volume relative to the matrix PS. The film specimens of the composite were prepared by solvent casting the suspensions described above using a small Teflon beaker and annealing at 150 °C under vacuum for one day.

### Methods

TEM observation of the CB dispersion state in a PS matrix on a micrometer scale was carried out by a JEOL101 instrument from JEOL Ltd. with an accelerating voltage of 80 kV at the Ultrastructural Research Center, Mie University. The 70-nm-thick specimens of the composite for TEM were fabricated by microtoming the solvent-cast films using an ULTRACUT E (Nisshin EM Co., Ltd.) with a glass knife. No additional staining was performed for the sample specimens.

USAXS and SAXS measurements were performed on the frontier soft-material beamline (FSBL) located at BL03XU [36], SPring-8, Hyogo, Japan. The camera length and wavelength, $\lambda$, of the X-ray were approximately 8 m and 0.2 nm for USAXS and approximately 2 m and 0.1 nm for SAXS. A PILUTUS 1M detector was used as a two-dimensional detector. The scattering intensity was measured by irradiating the X-ray beam along the direction perpendicular to the film surface. The CB powder sample was prepared for X-ray scattering by sandwiching sparse powder between Kapton tape. The isotropic scattering pattern was circularly averaged to obtain a scattering intensity, $I(q)$, profile as a function of the scattering vector, $q$, defined as $(4\pi/\lambda)\sin\theta$, where $2\theta$ is the scattering angle. The USAXS and SAXS intensity profiles were combined by only scaling the scattering intensity.

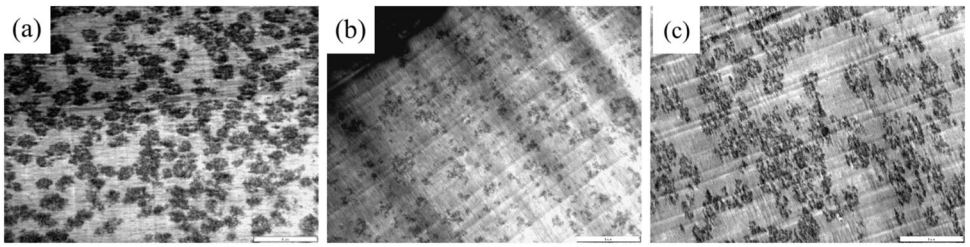


**Fig. 1** TEM images of PS composites with 2.7 vol% CB prepared by solvent casting suspensions in **a** chloroform, **b** THF, and **c** toluene. The length of the white bar in each image corresponds to 5 μm

The dynamic viscoelasticity measurements were conducted on a MCR302 (Anton Paar) instrument at the National Institute for Materials Science (NIMS), Tsukuba, Japan. The solvent-cast films were broken into small pieces, and then 1-mm-thick disk specimens with 8 mm $\phi$ were prepared for the rheology measurements by molding the film fragments at 170 °C under ~200 MPa for ~10 s. A parallel-plate with 8 mm $\phi$ was used, and the measurement was conducted at 150 °C with flowing dry nitrogen gas. The linear region at low strain was confirmed by strain sweep measurements at a low angular frequency, $\omega$, of 0.01 rad/s. The $\omega$ dependence of the storage, $G'$, and loss, $G''$, moduli was measured in a range of $\omega$ from 0.01 to 100 rad/s at a constant strain of 0.1%, which corresponds to the linear viscoelastic region.

## Results and discussion

The TEM images for solvent-cast films of PS composites with 2.7 vol% of CB from suspensions in different dispersion media are shown in Fig. 1. The dark regions in these images correspond to CB dispersed in the brighter regions of PS. CB is darker because the electron density of CB is higher than that of the matrix PS. Among the three dispersion media used here, CB was most uniformly dispersed in the composite prepared using THF. CB aggregates with relatively large sizes formed in the composites created from chloroform and toluene suspensions, and most of the added CB was localized in the lower part of the solvent-cast films. It should also be noted that the amount of CB in the composites from chloroform and toluene appeared to more than that from THF in the TEM images reflecting the suspension stability. The TEM images of the composites with 10 vol% CB content are not shown here, because the CB amount in the lower part of the films was too large to identify differences in the aggregate structure of CB produced by the dispersion medium. Bergin et al. [37] evaluated the dispersibility of single-walled carbon nanotubes in a range of dispersion media using the Hansen solubility parameter. The square of the Hildebrand solubility parameter, $\delta_T$, is equalized to the sum of the squares of dispersive, $\delta_d$, polar, $\delta_p$, and hydrogen bonding, $\delta_h$, solubility parameters.

$$\delta_T^2=\delta_d^2+\delta_p^2+\delta_h^2 \quad (1)$$

The solubility of a polymer or dispersibility of particles can be quantitatively evaluated by the distance in the Hansen space between the points of the polymer or particles (A) and the solvent (B),

$$R_{A,B}=\{(\delta_{d,A}-\delta_{d,B})^2+(\delta_{p,A}-\delta_{p,B})^2+(\delta_{h,A}-\delta_{h,B})^2\}^{1/2} \quad (2)$$

Generally, polymer solubility or particle dispersibility is higher for a solvent with a lower $R_{A,B}$. The Hansen solubility parameters, $\delta_d$, $\delta_p$, and $\delta_h$, for all components [38], and $R_{A,B}$ between PS or CB and the solvent calculated according to Eq. 2, are summarized in Table 1. It was found that the value of $R_{PS}$ is the highest for THF among the three solvents, implying that the solubility of PS is the lowest in THF; PS tends to adsorb physically on CB in a THF suspension. The $R_{CB}$ value is the lowest for THF, implying that its CB dispersibility is the highest among the three media. Thus, CB is expected to be most uniformly dispersed in the composite solvent cast from the THF suspension, since the CB dispersibility in the solvent is high and the physically adsorbed PS on CB prevents CB particles from flocculating in THF. The saturated adsorption amount of PS on CB in THF was evaluated to be ~0.09 g/g by a gravitational method and was the larger than that of the other two: ~0.05 g/g for both chloroform and toluene. In the other two dispersion media, CB dispersibility is low, and CB particles easily flocculate and settle in an early stage of solvent casting. The dispersion state of CB in the polymer reflects the suspension stability in the dispersion medium.

Figure 2 shows the combined USAXS and SAXS intensity profile, $I(q)$, for CB powder as a function of $q$. The $I(q)$ profile had a deflection point at ~0.2 $nm^{-1}$ in $q$, which corresponds to the size of the CB primary particle. The USAXS and SAXS profiles for the CB powder, which was sparsely sandwiched between Kapton tape, were well combined by simply adjusting a factor in the scattering intensities. Koga et al. [11] quantitatively analyzed the

aggregate structure of CB in rubber by using combined ultrasmall-angle and small-angle X-ray and neutron scattering techniques. The $I(q)$ profiles were analyzed by using a unified equation of Beaucage [11, 39]

$$I(q) = A\exp\left(-q^2R^2/3\right)q^{-D_m} + G\exp\left(-q^2R^2/3\right) + B\left[\mathrm{erf}\left(qR/6^{1/2}\right)\right]^{3(6-D_s)} q^{-(6-D_s)} \quad (3)$$

where $R$, $D_m$, and $D_s$ are the lower cutoff length of the mass fractal structure, and the mass and surface fractal dimensions, respectively, and $A$, $G$, and $B$ are proportional constants for each term in the equation. In principle, these proportional constants also reflect structural information. However, they were not utilized for the structural analysis in this study because the scattering intensity was not calibrated to an absolute scale. The solid line in the figure is the fitted curve using Eq. 3. The low $q$ upturn of the scattering intensities could be attributed to larger agglomerates of CB powder. The values of $R$, $D_m$, and $D_s$ for the CB powder were evaluated to be 10.05±0.12 nm, 2.437±0.043, and 2.651±0.014, respectively. The value of $R$ estimated by X-ray scattering was slightly lower than the primary particle diameter, 16 nm.

The $I(q)$ profiles for the PS composites with the addition of 2.7 and 10 vol% CB solvent-cast from suspensions in different dispersion media, i.e., chloroform, THF, and toluene, are shown in Figs 3 and 4, respectively. Each profile in the figures is shifted vertically for clarity. The USAXS and SAXS profiles for all the composites were well combined by simply adjusting a factor in the scattering intensities, as the CB powder shown above was. All the $I(q)$ profiles represented almost the same $q$ dependence irrespective of the dispersion medium. There is a deflection point of ~0.2 $nm^{-1}$ in $q$, and the scattering intensities are scaled with $q$ to the power of ~−2 and ~−3.7 below and above the deflection point, respectively. The scattering data for the composite films were analyzed by fitting with Eq. 3 and assuming that the heterogeneous dispersion of CB in the solvent-cast films along the depth direction, as observed in TEM images, does not affect the results since the heterogeneous distribution of CB could be averaged out in the scattering volume. The values of the structural parameters $R$, $D_m$, and $D_s$, evaluated using Eq. 3 are tabulated in Table 2. The size of the CB primary particle was evaluated to be 10–11 nm for the composites with 2.7 and 10 vol% CB, and this size is almost the same as that estimated for the CB powder. The $R$ value of CB in toluene or rubber evaluated by Koga et al. [11] was higher than that of a primary particle and corresponded to the aggregates composed of nine primary particles. The $D_m$ value for all the composites was lower than that for the CB powder; CB was well-dispersed by ultrasonication in the suspension. The $D_m$ value for the composites prepared using toluene was higher than that using chloroform irrespective of the CB content, but the difference in $D_m$ between 2.7 and 10 vol% CB was

**Table 1** The Hansen solubility parameters for the dispersive, polar and hydrogen-bonding components and the distance in the Hansen space between the points representing the solvent and PS or CB

| Materials | $\delta_d$ ($MPa^{1/2}$) | $\delta_p$ ($MPa^{1/2}$) | $\delta_h$ ($MPa^{1/2}$) | $\delta_T$ ($MPa^{1/2}$) | $R_{PS}$ ($MPa^{1/2}$) | $R_{CB}$ ($MPa^{1/2}$) |
|---|---|---|---|---|---|---|
| PS | 18.5 | 4.5 | 2.9 | 19.3 | – | – |
| CB | 21.1 | 12.3 | 11.3 | 26.9 | – | – |
| Chloroform | 17.8 | 3.1 | 5.7 | 18.9 | 3.2 | 11.3 |
| THF | 16.8 | 5.7 | 8.0 | 19.5 | 5.5 | 8.5 |
| Toluene | 18.0 | 1.4 | 2.0 | 18.2 | 3.3 | 14.7 |

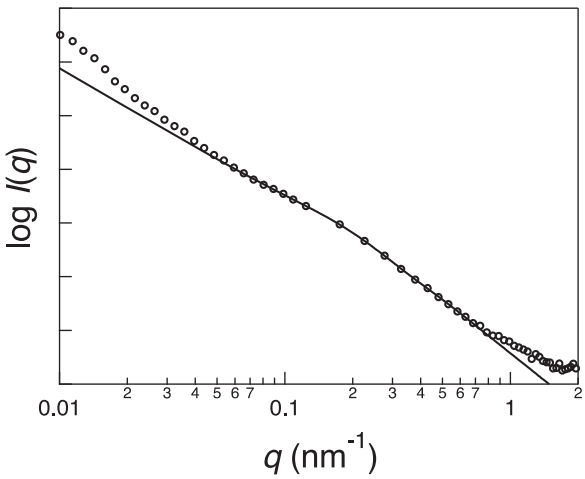


**Fig. 2** The combined USAXS and SAXS intensity profile for neat CB powder as a function of $q$. The solid line is the calculated profile using a unified Beaucage equation

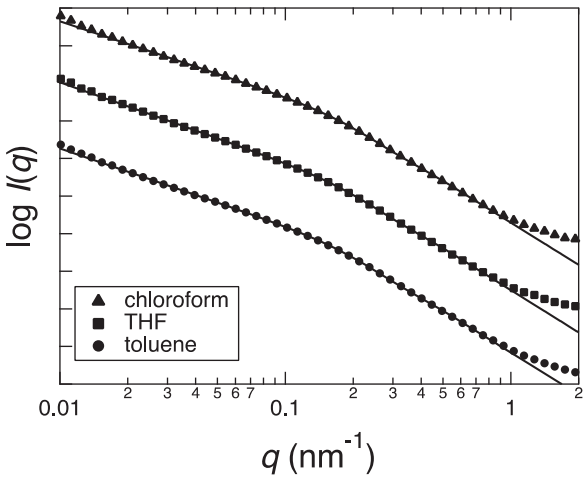


**Fig. 3** The combined USAXS and SAXS intensity profile for PS composites with 2.7 vol% CB content solvent cast from suspensions in chloroform, THF, and toluene

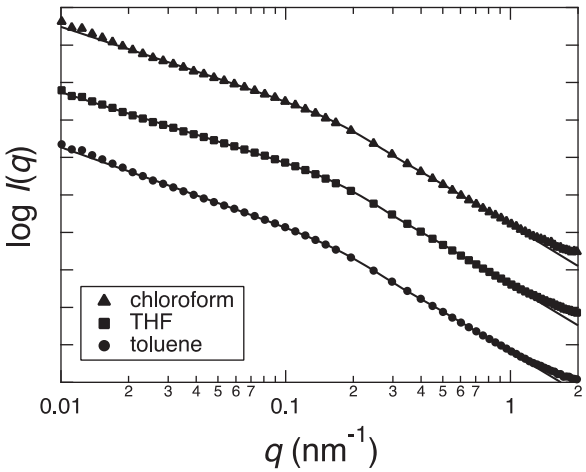


**Fig. 4** The combined USAXS and SAXS intensity profile for the PS composites with 10 vol% CB content prepared using different dispersion media

**Table 2** The structural parameters of CB dispersed in PS using different dispersion media

| 2.7 vol% | $R$ (nm) | $D_m$ | $D_s$ |
|---|---|---|---|
| Chloroform | 10.59 ± 0.04 | 1.993 ± 0.003 | 2.279 ± 0.004 |
| THF | 10.43 ± 0.05 | 2.117 ± 0.003 | 2.262 ± 0.004 |
| Toluene | 10.50 ± 0.03 | 2.049 ± 0.002 | 2.284 ± 0.003 |
| 10 vol% | $R$ (nm) | $D_m$ | $D_s$ |
| Chloroform | 10.55 ± 0.03 | 1.969 ± 0.003 | 2.333 ± 0.002 |
| THF | 10.85 ± 0.02 | 1.880 ± 0.003 | 2.363 ± 0.001 |
| Toluene | 10.71 ± 0.03 | 2.117 ± 0.002 | 2.355 ± 0.002 |

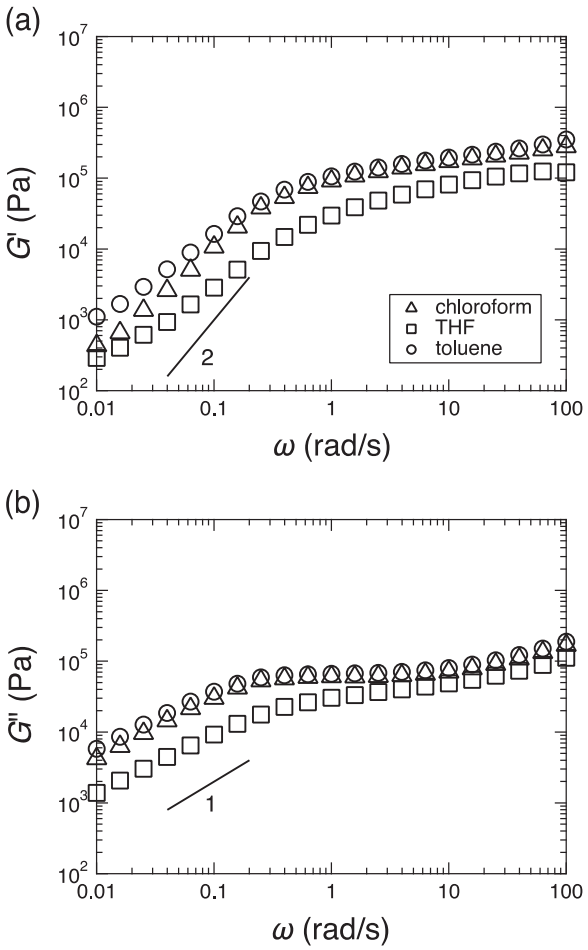


**Fig. 5** The angular frequency dependence of **a** storage and **b** loss moduli of the PS composites with 2.7 vol% CB prepared using chloroform, THF, and toluene as the dispersion medium for the suspension

relatively large in the composites prepared using THF. A dispersion medium with a higher $R_{CB}$, which implies lower CB dispersibility in suspension, could lead to CB aggregates with a higher $D_m$ value. However, the $D_s$ value was independent of the dispersion medium, but a higher CB content exhibited a higher $D_s$ value. The $D_s$ values evaluated for the composites were clearly lower than those for the CB powder. This could be ascribed to the effects of physical adsorption of the polymer on the CB surface.

Figure 5a, b show the $\omega$ dependence of $G'$ and $G''$, respectively, at 150 °C for the composites with 2.7 vol% CB content prepared using different dispersion media for a $\omega$ range from 0.01 to 100 rad/s. The viscoelastic moduli of the composites with 2.7 vol% CB exhibited almost the same frequency dependence irrespective of the dispersion medium used for preparing the suspension. The moduli of matrix PS without CB prepared by the same procedure used for the composites followed typical Maxwellian behavior, in which $G'$ and $G''$ scale with $\omega^2$ and $\omega^1$, respectively, in a low $\omega$ region. The elastic moduli of the composites had a slightly weaker $\omega$ dependence than that of PS in the low $\omega$ region, implying that the CB content is still below the critical value of the percolation limit, while their loss moduli had almost the same dependence on $\omega$ as that of PS. Unfortunately, an absolute comparison of the composite modulus with that of PS is not possible with the data obtained here since the composite moduli were almost equal to or lower than that of PS. These data are not shown here. It has been reported that the viscoelastic moduli of composites of PS or poly(ethylene oxide) with fumed silica are higher than that of the neat polymer and that these values increase with increasing silica content over the whole range of angular frequencies [31]. This discrepancy could be attributed to the heterogeneous dispersion of CB in the composite film produced by the solvent-casting method adopted in this study. As shown above, TEM observations revealed that CB was heterogeneously distributed in the lower part of the solvent-cast films. In this study, no further annealing of the rheological-measurement disk specimens

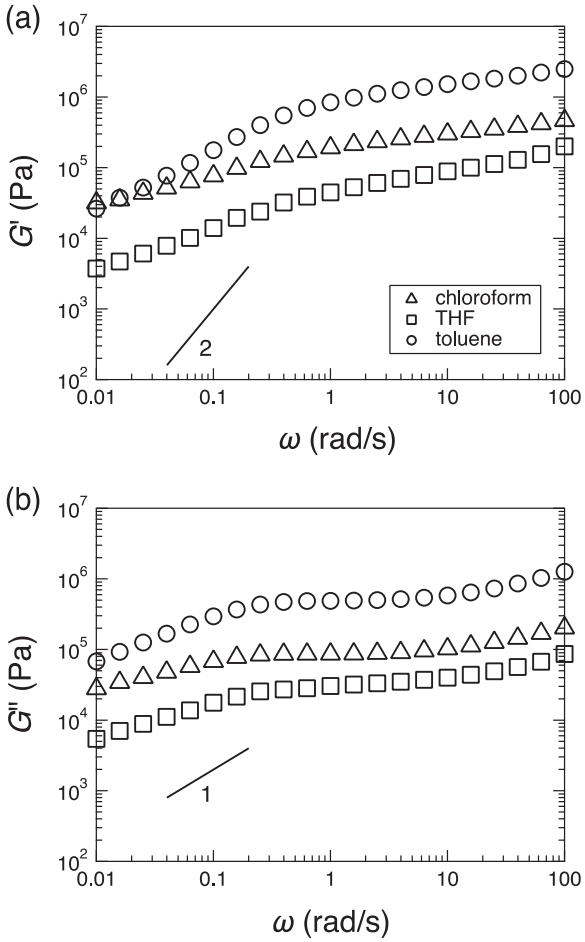


**Fig. 6** The angular frequency dependence of **a** storage and **b** loss moduli of the PS composites with 10 vol% CB prepared using different dispersion media for the suspension

was conducted after molding at 170 °C, and the time evolution of the modulus was not confirmed to investigate the inherent effects of the CB dispersion state produced by the difference in dispersion media. This heterogeneous dispersion of CB in the composite films may result in the difference between the composites and pure PS without heterogeneity. Thus, we believe that a comparison of the viscoelasticity among the composites could be meaningful and may reflect the difference in the aggregate structure as well as the dispersion state of CB. The modulus for the composite prepared from toluene was the highest and that of the composite prepared from THF was the lowest with the same CB content. The rheological results for the composites with 10 vol% CB are shown in Fig. 6. Both viscoelastic moduli were higher than those for the composites with lower CB content. The frequency dependence of $G'$ was much weaker than that expected from Maxwellian behavior, implying that the CB content exceeds the percolation limit. For the composites with 10 vol% CB content, the viscoelasticity also varied according to the dispersion medium, as observed for the lower CB content. Zhao et al. reported that the shape, connectivity, and structural openness of particles affect the viscoelastic properties of a polymer composite [40]. The viscoelasticity of a polymer composite is largely influenced by the macroscopic dispersion state and aggregate structure of CB induced by the dispersion medium.

## Conclusion

The dispersion state and aggregate structure of CB in PS composites prepared by solvent casting suspensions in different dispersion media were investigated using TEM and small-angle X-ray scattering techniques. The macroscopic dispersion state of CB in the polymer was affected by the dispersion medium used for the sample preparation, reflecting the suspension stability. CB was more or less heterogeneously distributed in the solvent-cast films along the depth direction. The mass fractal dimension of CB in the composite films, which was evaluated by small-angle X-ray scattering with a spatial resolution of nanometers, tended to exhibit a higher value for a dispersion medium with less CB dispersibility. The surface fractal dimension of CB in the composites was lower than that of the CB powder due to the effect of physical adsorption of the polymer on the CB surface. Furthermore, the viscoelastic moduli of the melt polymer composites below and above the percolation limit varied with the dispersion medium, reflecting the difference in the macroscopic dispersion state and aggregate structure of CB in polystyrene.

**Acknowledgements** The USAXS and SAXS measurements were conducted on the frontier soft-material beamline (FSBL) located at BL03XU, SPring-8, with approval for the proposals of 2016A7206, 2016B7256, 2017A7205, and 2017B7257. We are very thankful to Dr. Hiroyasu Masunaga of Japan Synchrotron Radiation Research Institute (JASRI) for his technical support on USAXS and SAXS measurements at FSBL. The dynamic viscoelasticity measurements in this study were supported by the NIMS Joint Research Hub Program. We are very indebted to Mr. Satoru Ogawa of Ultrastructural Research Center, Mie University and Ms. Yukiko Fujita, Faculty of Engineering, Mie University for their technical support on microtoming and TEM observation on the PS composites with CB. This study was partly supported by a Grant-in-Aid for Scientific Research (C) (24550252) of the Ministry of Education, Culture, Science, Sports and Technology, Japan.

## Compliance with ethical standards

**Conflict of interest** The authors declare that they have no conflict of interest.

## References


1. Jancar J, Douglas JF, Starr FW, Kumar SK, Cassagnau P, Lesser AJ, et al. Current issues in research on structure-property relationships in polymer nanocomposites. Polymer. 2010;51: 3321–43.
2. Kumar SK, Benicewicz BC, Vaia RA, Winey KI. 50th Anniversary perspective: are polymer nanocomposites practical for applications? Macromolecules. 2017;50:714–31.
3. Neutrons, X-rays and light, scattering methods applied to soft condensed matter. Lindner P, Zemb Th, editors. Amsterdam, the Netherlands: Elsevier B.V.; 2002.
4. Schaefer DW, Justice RS. How nano are nanocomposites? Macromolecules. 2007;40:8501–17.
5. Kawaguchi M, Kimura Y, Tanahashi T, Takeoka J, Kato T, Suzuki J, et al. Polymer adsorption effects on structures and rheological properties of silica suspensions. Langmuir. 1995;11:563–7.
6. Kawaguchi M, Mizutani A, Matsushita Y, Kato T. Molecular weight dependence of structures and rheological properties for fumed silica suspensions in polystyrene solutions. Langmuir. 1996;12:6179–83.
7. Rieker TP, Misono S, Ehrburger-Dolle F. Small-angle X-ray scattering from carbon blacks: crossover between the fractal and Porod regimes. Langmuir. 1999;15:914–7.
8. Rieker TP, Hindermann-Bischoff M, Ehrburger-Dolle F. Small-angle X-ray scattering study of the morphology of carbon blacks mass fractal aggregates in polymeric composites. Langmuir. 2000;16:5588–92.
9. Kammler HK, Beaucage G, Mueller R, Pratsinis SE. Structure of flame-made silica nanoparticles by ultra-small-angle X-ray scattering. Langmuir. 2004;20:1915–21.
10. Koga T, Takenaka M, Aizawa K, Nakamura M, Hashimoto T. Structure factors of dispersible units of carbon black filler in rubbers. Langmuir. 2005;21:11409–13.
11. Koga T, Hashimoto T, Takenaka M, Aizawa K, Amino N, Nakamura M, et al. New insight into hierarchical structures of carbon black dispersed in polymer matrices: A combined small-angle scattering study. Macromolecules. 2008;41:453–64.
12. Jouault N, Vallat P, Dalmas F, Said S, Jestin J, Boue F. Well-dispersed fractal aggregates as filler in polymer-silica nanocomposites: long-range effects in rheology. Macromolecules. 2009;42:2031–40.
13. Jouault N, Dalmas F, Boue F, Jestin J. Multiscale characterization of filler dispersion and origins of mechanical reinforcement in model nanocomposites. Polymer. 2012;53:761–75.
14. Qiu D, Dreiss CA, Cosgrove T, Howe AM. Small-angle neutron scattering study of concentrated colloidal dispersions: the interparticle interactions between sterically stabilized particles. Langmuir. 2005;21:9964–9.
15. Qiu D, Cosgrove T, Howe AM. Small-angle neutron scattering study of concentrated colloidal dispersions: The electrostatic/steric composite interactions between colloidal particles. Langmuir. 2006;22:6060–7.
16. Qiu D, Cosgrove T, Howe AM. Steric interactions between physically adsorbed polymer-coated colloidal particles: soft or hard? Langmuir. 2007;23:475–81.
17. Qiu D, Flood C, Cosgrove T. A small-angle neutron scattering study of adsorbed polymer structure in concentrated colloidal dispersions. Langmuir. 2008;24:2983–6.
18. Takenaka M, Nishitsuji S, Amino N, Ishikawa Y, Yamaguchi D, Koizumi S. Structure analyses of swollen rubber-filler systems by using contrast variation SANS. Macromolecules. 2009;42:308–11.
19. Liu D, Chen J, Song L, Lu A, Wang Y, Sun G. Parameterization of silica-filled silicone rubber morphology: a contrast variation SANS and TEM study. Polymer. 2017;120:155–63.
20. de Kruif CG, van Iersel EMF, Vrij A, Russel WB. Hard sphere colloidal dispersions. Viscosity as a function of shear rate and volume fraction. J Chem Phys. 1986;83:4717–25.
21. Trappe V, Weitz DA. Scaling of the viscoelasticity of weakly attractive particles. Phys Rev Lett. 2000;85:449–52.
22. Prasad V, Trappe V, Dinsmore AD, Segre PN, Cipelletti L, Weitz DA. Universal features of the fluid to solid transition for attractive colloidal particles. Faraday Discuss. 2003;123:1–12.
23. Gleissle W, Hochstein B. Validity of the Cox-Merz rule for concentrated suspensions. J Rheol. 2003;47:897–910.
24. Zhang Q, Archer LA. Poly(ethylene oxide)/silica nanocomposites: structure and rheology. Langmuir. 2002;18:10435–42.
25. Anderson BJ, Zukoski CF. Rheology and microstructure of an unentangled polymer nanocomposite melt. Macromolecules. 2008;41:9326–34.
26. Anderson BJ, Zukoski CF. Rheology and microstructure of entangled polymer nanocomposite melts. Macromolecules. 2009;42:8370–84.
27. Anderson BJ, Zukoski CF. Rheology and microstructure of polymer nanocomposite melts: variation of polymer segment-surface interaction. Langmuir. 2010;26:8709–20.
28. Romeo G, Filippone G, Fernandez-Nieves A, Russo P, Acierno D. Elasticity and dynamics of particle gels in non-Newtonian melts. Rheol Acta. 2008;47:989–97.
29. Filippone G, Romeo G, Acierno D. Viscoelasticity and structure of polystyrene/fumed silica nanocomposites: filler network and hydrodynamic contributions. Langmuir. 2010;26: 2714–20.
30. Filippone G, de Luna MS. A unifying approach for the linear viscoelasticity of polymer nanocomposites. Macromolecules. 2012;45:8853–60.
31. Capuano G, Filippone G, Romeo G, Acierno D. Universal features of the melt elasticity of interacting polymer nanocomposites. Langmuir. 2012;28:5458–63.
32. Song Y, Zheng Q. Concepts and conflicts in nanoparticles reinforcement to polymers beyond hydrodynamics. Prog Mater Sci. 2016;84:1–58.
33. Song Y, Tan Y, Zheng Q. Linear rheology of carbon black filled polystyrene. Polymer. 2017;112:35–42.
34. Russel WB, Saville DA, Schowalter WR. Colloidal dispersion. New York: Cambridge University Press; 1989.
35. McFarlane NL, Wagner NJ, Kaler EW, Lynch ML. Poly(ethylene oxide) (PEO) and poly(vinyl pyrolidone) (PVP) induce different changes in the colloid stability of nanoparticles. Langmuir. 2010;26:13823–30.
36. Masunaga H, Ogawa H, Takano T, Sasaki S, Goto S, Tanaka T, et al. Multipurpose soft-material SAXS/WAXS/GISAXS beamline at SPring-8. Polym J. 2011;43:471–7.
37. Bergin SD, Sun Z, Rickard D, Streich PV, Hamilton JP, Coleman JN. Multicomponent solubility parameters for single-walled carbon nanotube-solvent mixtures. ACS Nano. 2009;3:2340–50.
38. Hansen CM. Hansen solubility parameters – a user's handbook. Boca Raton, FL: CRC Press; 2007.
39. Beaucage G. Approximations leading to a unified exponential/power-law approach to small-angle scattering. J Appl Cryst. 1995;28:717–28.
40. Zhao D, Ge S, Senses E, Akcora P, Jestin J, Kumar SK. Role of filler shape and connectivity on the viscoelastic behavior in polymer nanocomposites. Macromolecules. 2015;48:5433–8.